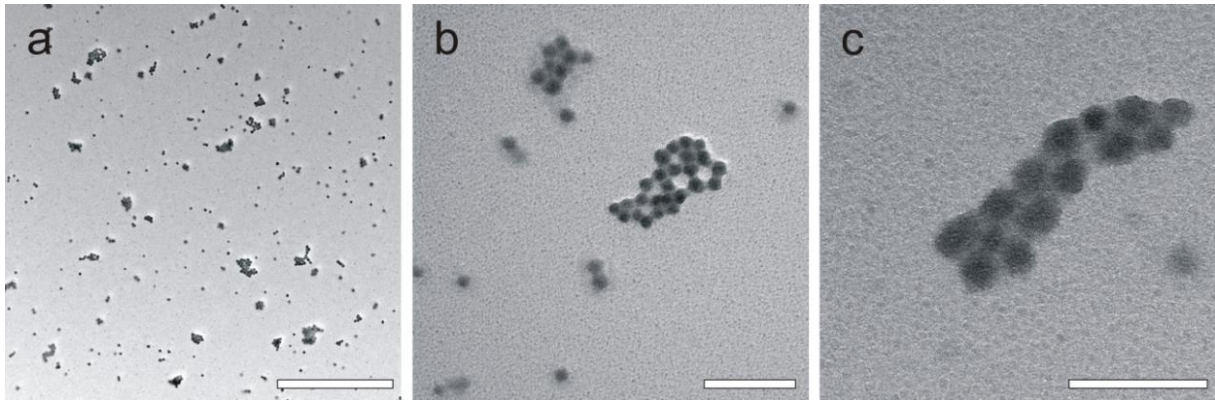
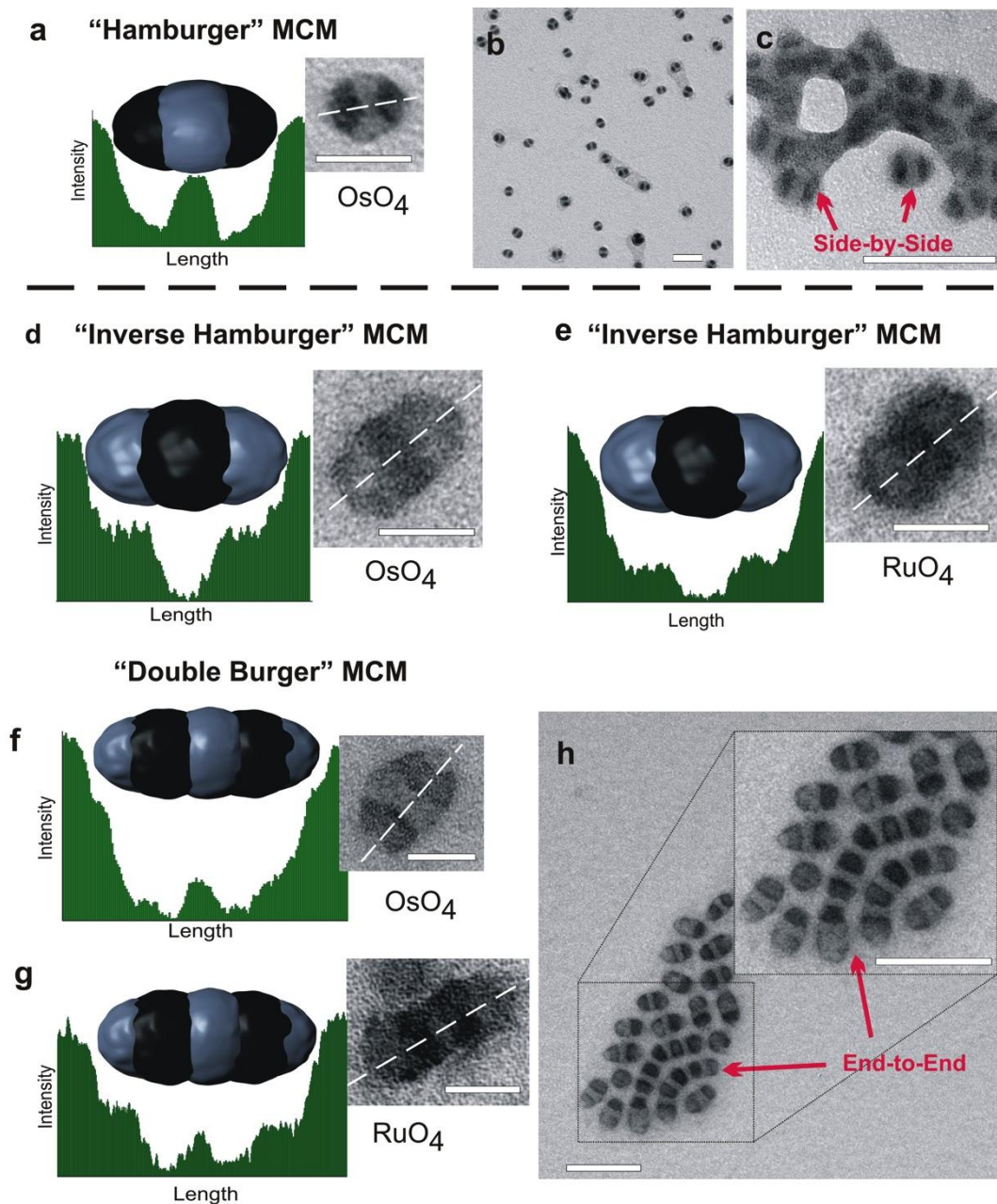


**Supplementary Figure S1. Dynamic light scattering CONTIN plots of subunits and corresponding spherical MCMs of polystyrene-*block*-polybutadiene-*block*-poly(methyl methacrylate) triblock terpolymers (SBM3-6).** In DMAC, well-defined subunits with hydrodynamic radii in the range of  $R_{h,app} = 11 \text{ nm} - 14 \text{ nm}$  can be found (left column). A clear shift in the dimensions is observed after dialysis against acetone/isopropanol (60/40 v/v) with values ranging from  $R_{h,app} = 36 \text{ nm} - 54 \text{ nm}$ , depending on the morphology of the formed spherical MCMs (middle column). The absence of an angular dependence of the DLS data by plotting the reduced decay rate,  $\Gamma/q^2$ , as a function of the squared scattering vector,  $q^2$ , and almost constant values for  $\Gamma/q^2$  in all cases confirm spherical MCMs with very narrow size distribution (right column). Polydispersity and anisometry typically lead to the observation of a curved plot (see Supplementary Figure S4, see also Supplementary Table S1 for terpolymer characteristics).

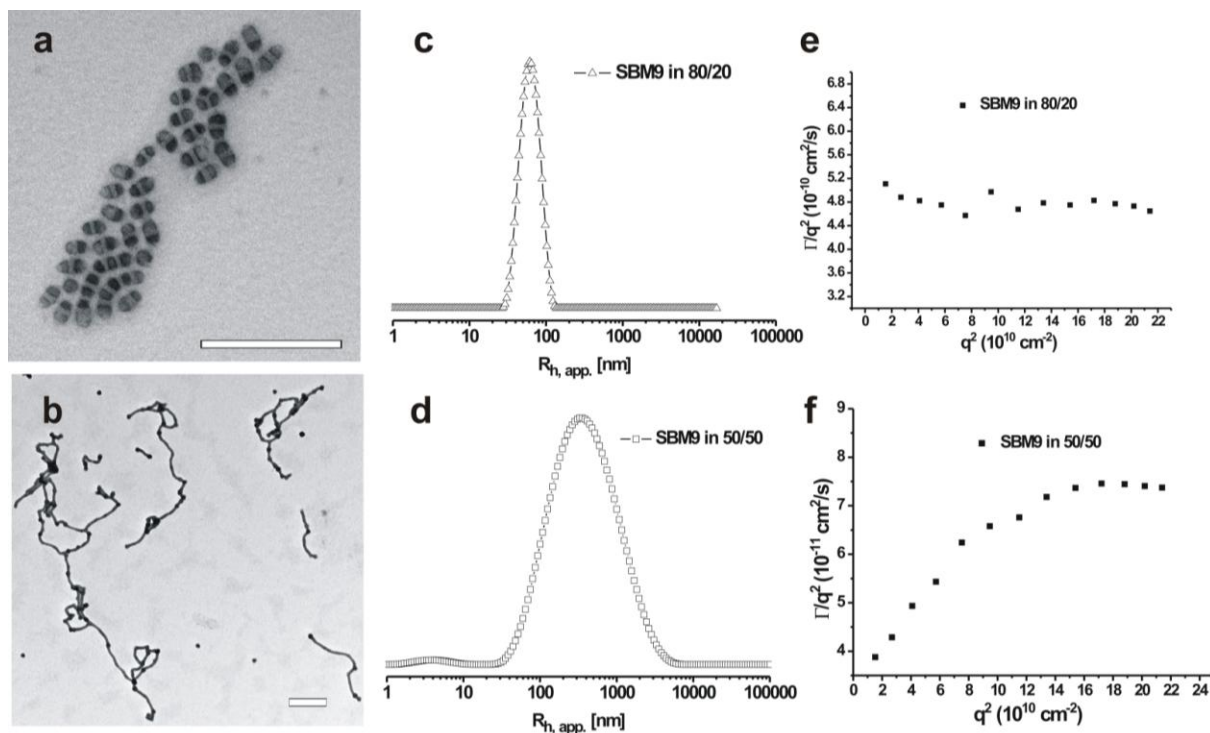


**Supplementary Figure S2. Influence of core mobility on MCM formation as demonstrated by crosslinking of the subunits.** To investigate the importance of a dynamic core, the PB cores of SBM9 micellar subunits were crosslinked in DMAc with the photo-crosslinker 2,4,6-trimethylbenzoyldiphenylphosphine oxide (Lucirin TPO<sup>®</sup>,  $\lambda_{\text{max}} = 360\text{nm}$ , obtained from BASF SE) by UV irradiation for 1 h. Any corona restructuring (i.e. refinement) during the aggregation of the subunits also requires a drastic rearrangement of chains in the micellar core. **(a-c)** After cross-linking in DMAc and subsequent dialysis into acetone/isopropanol (60/40 v/v), no defined MCMs can be observed (TEM images, OsO<sub>4</sub> stained with increasing magnification; scale bars are 1  $\mu\text{m}$  **(a)**, 200 nm **(b)**, 100 nm **(c)**). For comparison, SBM9 forms well-defined mesoscale colloidal polymers in this solvent mixture without crosslinking (see Figure 4e,f and Figure 5a-d in the main text). Those can clearly not be found. Instead, core crosslinked micelles and their ill-defined aggregates appear. This clearly demonstrates that the presence of a dynamic core during structural rearrangements and fusion of subunits into final MCMs is necessary. Large-scale corona restructuring is only possible for dynamic cores.

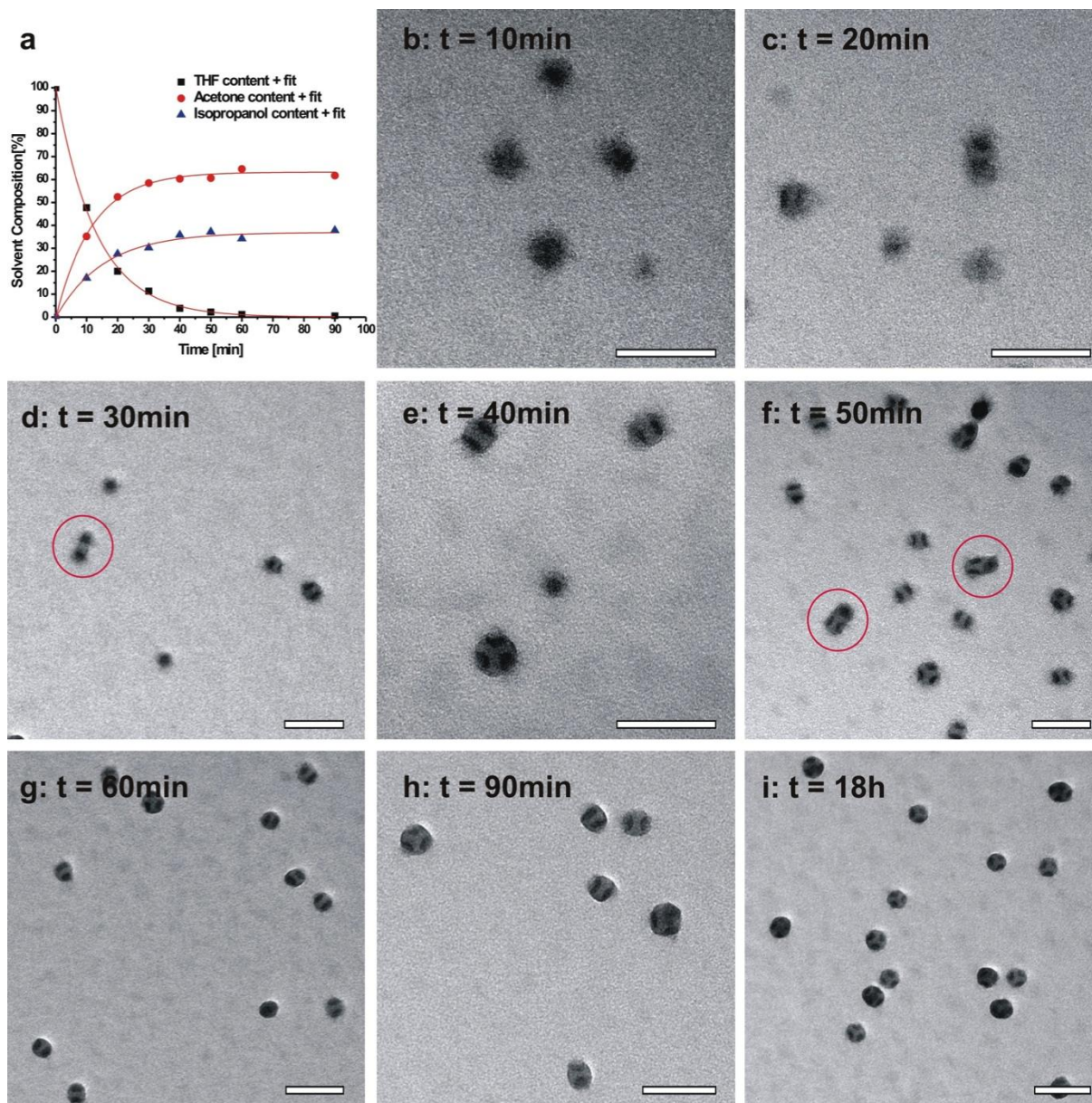


**Supplementary Figure S3. Structural differences in "hamburger" (BSB), "inverse hamburger" (SBS) and "double burger" (SBS)<sub>2</sub> MCMs as decisive building blocks to understand the polymerization of "double-burger" vs. the aggregation of "hamburger" MCMs. (a) "Hamburger" MCMs possess terminal compartments of PB from which corona chains emanate and are thus incapable of end-to-end growth. Grey-scale analysis clearly shows that "hamburger" MCMs exhibit dark terminal PB compartments after which the intensity (contrast) immediately levels off to the underlying carbon film of the TEM grid (OsO<sub>4</sub> stained; PMMA is not visible due to e-beam degradation; scale bar is 50 nm). (b) Overview of "hamburger" MCMs (scale bar is 100 nm). (c) A contracting corona can only lead to aggregation along the middle compartment of PS, thus favoring side-by-side assembly observed depositing a more concentrated solution on the TEM grid (scale bar is 200 nm). (d-e) Grey-scale analysis of "inverse hamburger" MCMs (scale bar is 50nm) and (f-g) "double-burger" MCMs that clearly show terminal PS compartments after OsO<sub>4</sub> and RuO<sub>4</sub> staining from which no stabilizing corona chains protrude (scale bars are 200 nm and 100 nm in insets). Terminal PS compartments become darker when stained with RuO<sub>4</sub>. RuO<sub>4</sub> stains both PS and PB, whereas OsO<sub>4</sub> only stains PB. "Double burgers" form**

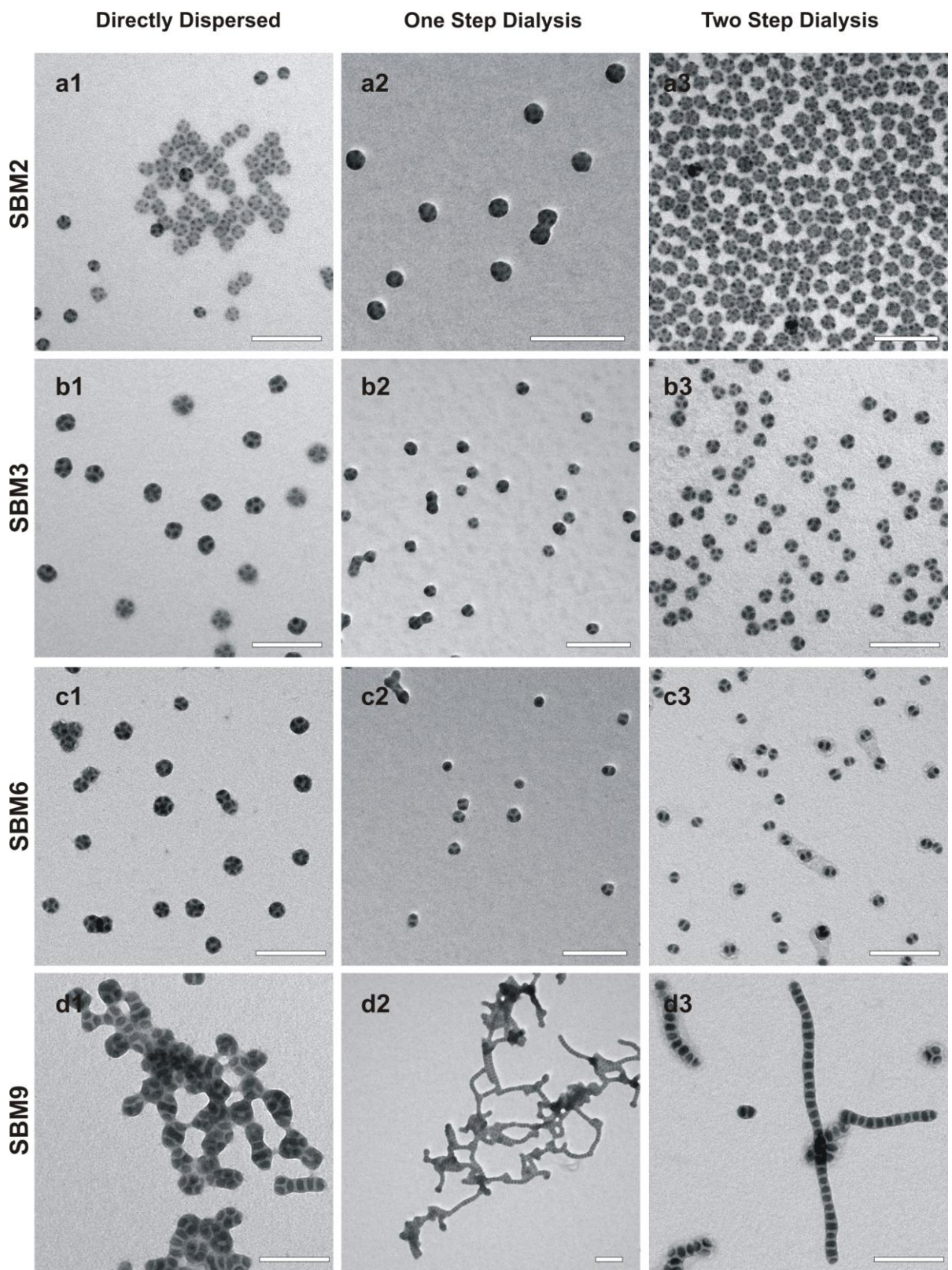
upon dimerization of “inverse hamburger” MCMs. Here, a small step in the grey-scale analysis can be observed before the intensity levels off to the background of the carbon coating, thus confirming the presence of terminal PS compartments. Note also the unusual non-spherical shape of the black polybutadiene compartments. Hence, these combined staining efforts unambiguously demonstrate the structural differences between BSB “hamburger” and SBS “inverse hamburgers” as well as their dimerized  $(SBS)_2 = SBSBS$  “double-burger” analogues. **(h)** Longitudinal end-to-end aggregation of “double-burger” MCMs. See also the extension of the concept of supramicellar polymers to TCD, which provides additional convincing imaging data for the aggregation of “inverse hamburgers” into “double-burgers” and subsequent end-to-end polymerization into colloidal chains (Fig. 6d-f in the main article). Therein, the pH allows tuning the corona volume and enables the observation of various intermediates via changing the acidity.



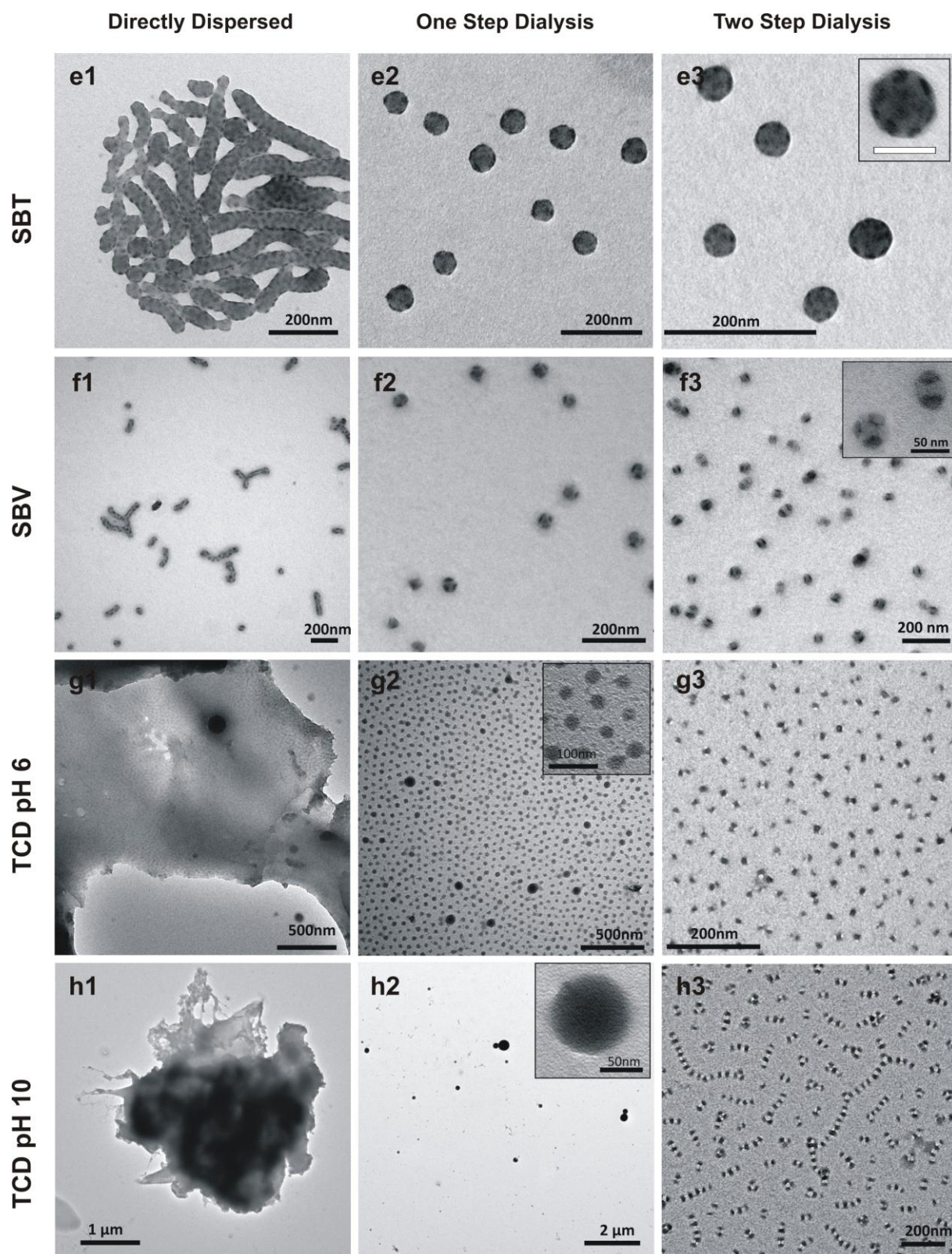
**Supplementary Figure S4. Supporting DLS for step-growth polymerization of SBM9. (a, c, e)** “Double-burger” MCMs are the dominant species according to DLS and TEM in acetone/isopropanol (80/20 v/v). **(b, d, f)** Colloidal mesoscale polymers formed by the polymerization of “double-burger” MCMs in acetone/isopropanol (50/50 v/v). **(a, b)** Transition from “double-burger” MCMs in acetone/isopropanol (80/20 v/v) to long segmented chains in acetone/isopropanol (50/50 v/v) observed in TEM (OsO<sub>4</sub> stained; scale bars are 500 nm). **(c, d)** DLS CONTIN plots at 90° allow following the mesoscale step-growth polymerization of “double-burgers” in-situ in solution and thus, excluding the possibility of colloidal polymers being drying artifacts in TEM. The transition from initial subunits in DMAc to MCMs and their subsequent step-growth polymerization is accompanied by a consecutive increase in hydrodynamic radius. The small  $R_{h,app} = 12 \pm 5$  nm of the subunits in DMAc (data not shown) increases about sevenfold to  $R_{h,app} = 61 \pm 17$  nm for the state of the “double-burger” MCMs in acetone/isopropanol (80/20 v/v). **(e, f)** Reduced decay rate,  $\Gamma/q^2$ , as a function of the squared scattering vector,  $q^2$ , for SBM9 at two different acetone/isopropanol solvent compositions. **(e)** The angular dependence of the DLS data is very weak, thus confirming near spherical “double-burger” MCMs in acetone/isopropanol (80/20 v/v). **(f)** Upon a further decrease of the solvent quality, step-growth polymerization into supra-colloidal worms is triggered and leads to higher values for  $R_{h,app, q \rightarrow 0} > 1000$  nm. In case of chain-like colloidal assemblies, additional rotational and bending modes contribute to the distribution of relaxation times, resulting in an observation of a dependence of the decay rate,  $\Gamma/q^2$ , on the squared scattering vector,  $q^2$ . In consequence, the strongly curved plot suggests the presence of long, non-spherical objects in acetone/isopropanol (50/50 v/v).



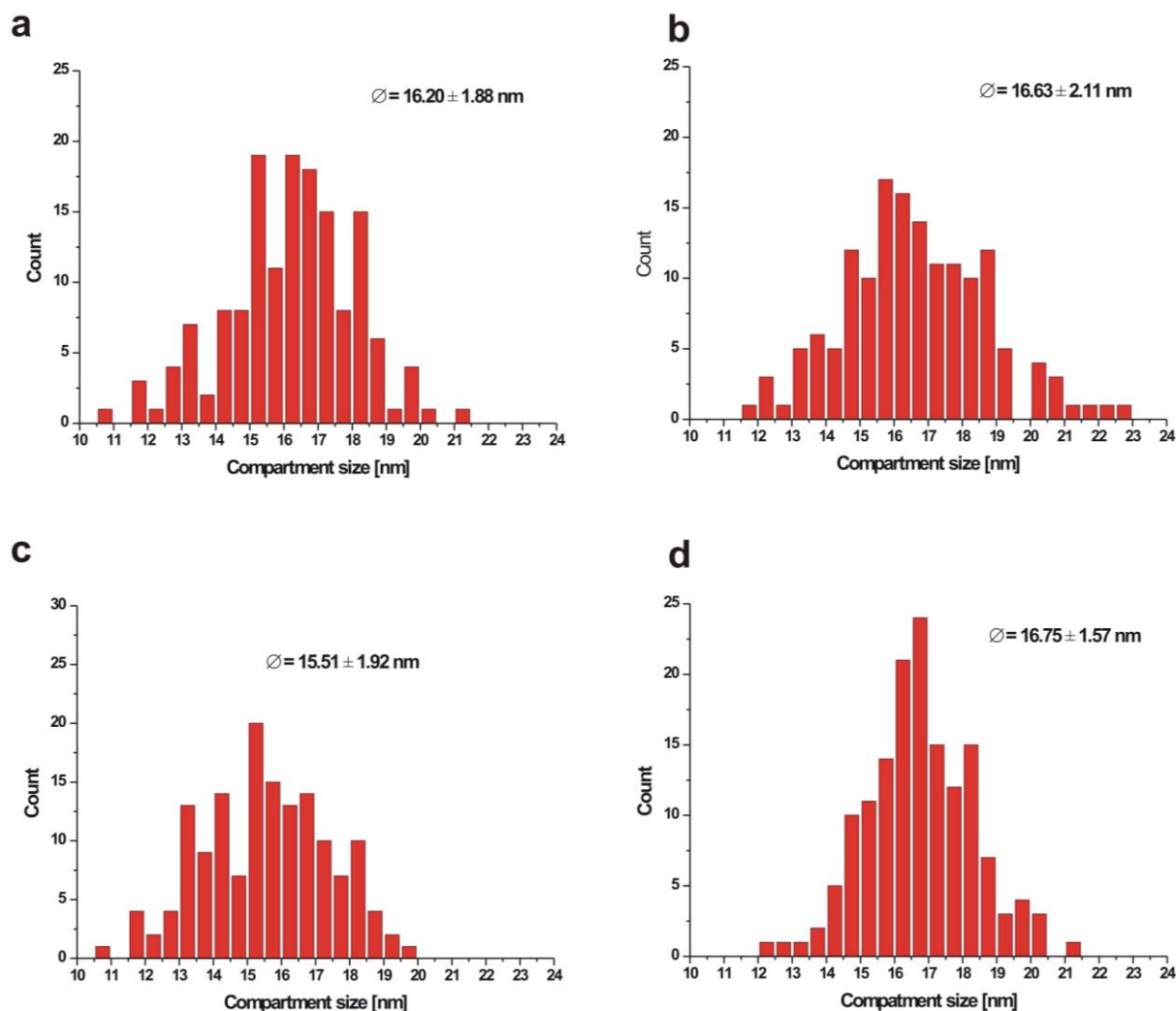
**Supplementary Figure S5. Kinetic study of SBM3 MCM formation by a one step dialysis from THF into acetone/isopropanol (60/40 v/v).** (a)  $^1\text{H}$ -NMR study of the time dependent solvent composition. (b-i) TEM micrographs of samples after specific time intervals as indicated within the figure (all samples were  $\text{OsO}_4$  stained; scale bar corresponds to 100 nm). The red circles highlight fusion events of subunits during the assembly (see also Supplementary Note 1).



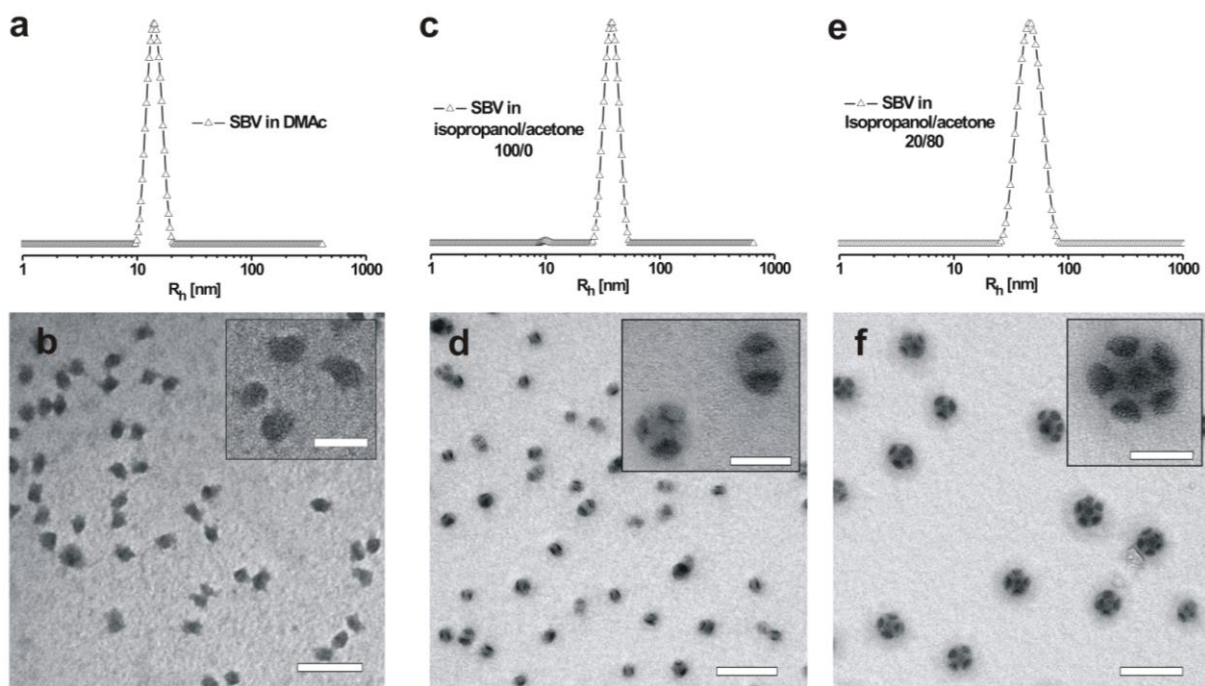
(Supplementary Figure S6, continued on the next page)



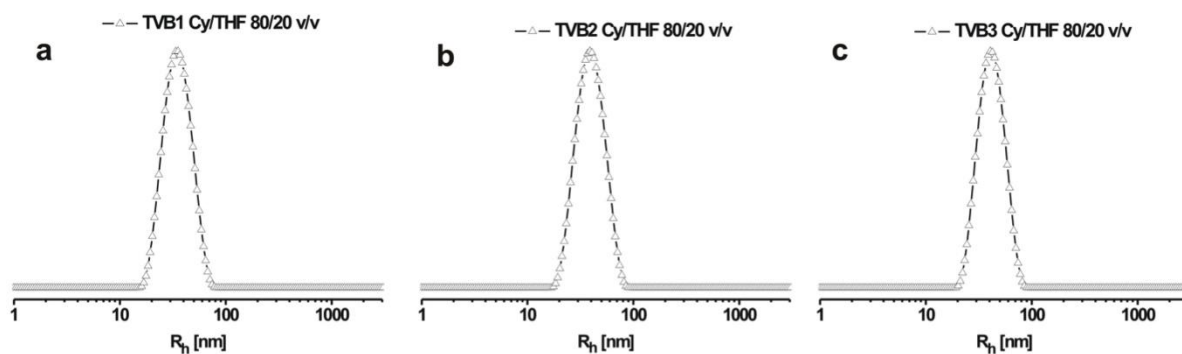
**Supplementary Figure S6. Terpolymer MCMs directly dispersed, prepared by one step dialysis, and via two step dialysis. (a1-a3) SBM2 "football" MCMs, (b1-b3) SBM3 "clover" MCMs, (c1-c3) SBM6 "hamburger" MCMs and (d1-d3) SBM9 worm-like micelles. (e1-e3) SBT "football" MCMs, (f1-f3) SBV "clover" MCMs, (g1-g3) TCD at pH = 6 oligomers, (h1-h3) TCD at pH = 10 worm-like MCMs (see also Supplementary Note 2).**



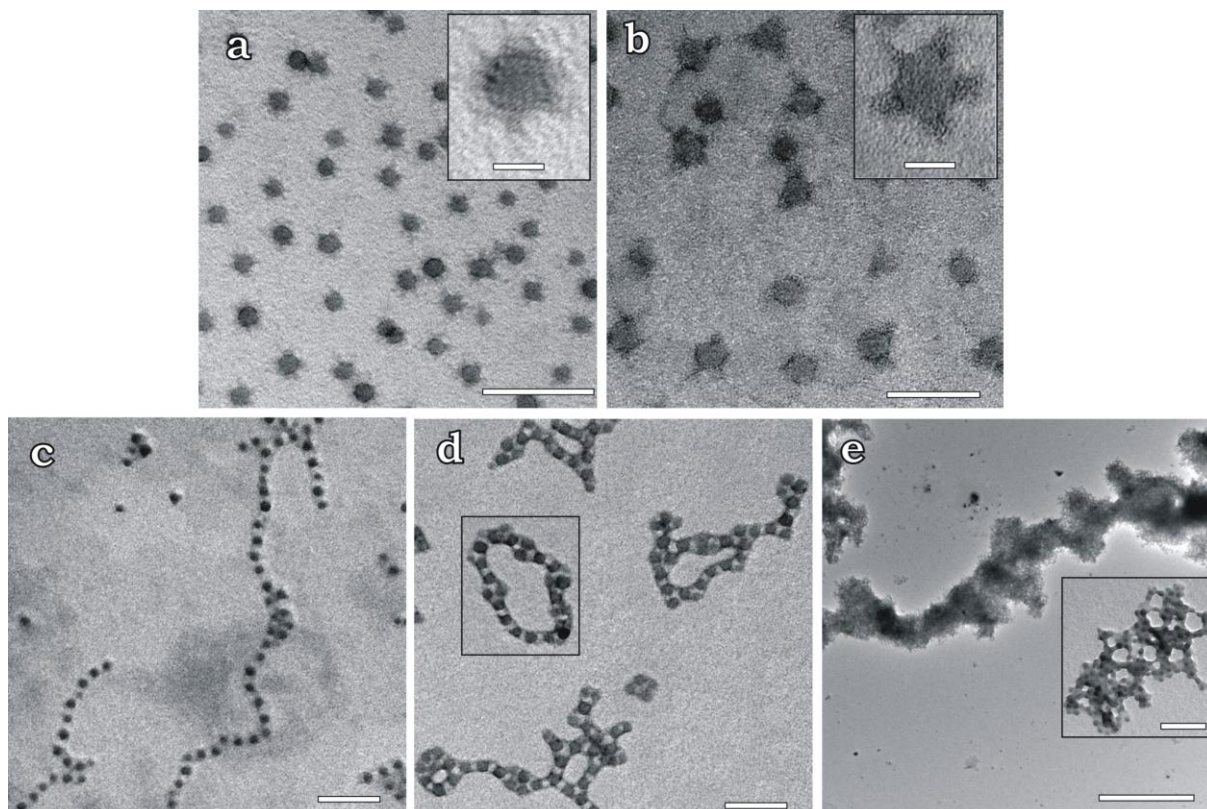
**Supplementary Figure S7. Statistical evaluation of compartment size distributions of PB patches of SBM3 MCMs during in-situ switching of aggregate morphologies with changing acetone/isopropanol content. (a)** Core diameters of  $16.2 \pm 1.9$  nm observed for subunits in acetone/isopropanol 90/10 v/v. **(b)** Compartment diameters of  $16.3 \pm 2.1$  nm of "hamburger" MCMs observed in 80/20 v/v, **(c)**  $15.5 \pm 1.9$  nm of "clover" MCMs in 60/40 v/v and **(d)**  $16.8 \pm 1.6$  nm of "football" MCMs in 50/50 v/v. At least 150 patches were evaluated for each sample. The number average diameters of the PB patches are in the range of  $16.1 \pm 0.6$  nm for all structures, thus nearly constant. Considering the slightly different geometries of the PB domains (spherical in subunits vs. elliptic in MCMs) and the unlike swelling in the various solvent mixtures, the uniformity strongly suggests exchange/assembly of intact subunits. Fusion and fission of PB domains as well as exchange of unimeric polymer molecules would result in larger differences.



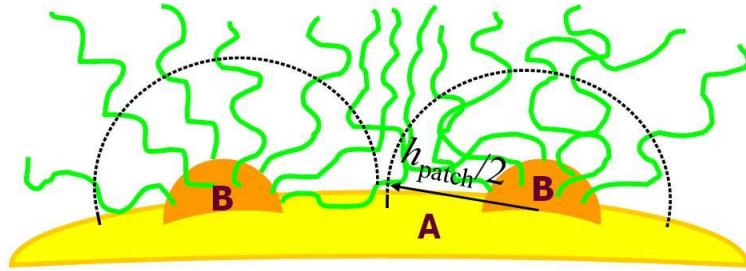
**Supplementary Figure S8. DLS CONTIN plots of polystyrene-*b*-polybutadiene-*b*-poly(2-vinylpyridine) (SBV) triblock terpolymer measured at an angle of 90° as well as respective TEM images (OsO<sub>4</sub> stained). (a, b) DLS confirms the presence of subunits in DMAc with  $R_{h,app} = 16 \pm 2$  nm. (c, d) After dialysis into isopropanol, MCMs with an increased radius of  $R_{h,app} = 36 \pm 7$  nm can be found. The slightly asymmetric ratio  $V_{PS}/V_{PB} = 1.67$  explains the formation of “hamburger” or “clover” MCMs. Both species are almost equally represented. (e, f) MCMs after dialysis against isopropanol/acetone (20/80 v/v). Addition of acetone leads to corona contraction and to an increased amount of subunits (5-6) per MCM and, in addition, to a larger hydrodynamic radius of  $R_{h,app} = 46 \pm 10$  nm. These observations are in good agreement with the results obtained earlier for SBM terpolymers of varying composition.**



**Supplementary Figure S9. CONTIN plots of poly(*tert*-butyl methacrylate)-*b*-poly(2-vinylpyridine)-*b*-polybutadiene (TVB1-3) terpolymer subunits in cyclohexane/THF (80/20 v/v) measured at an angle of 90°. (a) TVB1 with  $R_{h,app} = 35 \pm 10$  nm, (b) TVB2 with  $R_{h,app} = 39 \pm 8$  nm and (c) TVB3 with  $R_{h,app} = 41 \pm 9$  nm. All TVB block terpolymers were synthesized via sequential living anionic polymerization starting with butadiene, followed by the addition of 2-vinylpyridine and *tert*-butyl methacrylate<sup>57</sup>. We changed the typical acronym sequence from BVT to TVB, as PB acts as the corona in this case. The characteristics of TVB1-3 are summarized in Table S1. TVB features a very polar and high  $T_g$  middle block, for which MCMs with a PB corona can be formed in non-polar solvents such as hydrocarbons (dodecane). The preceding subunits with P2VP core and PtBMA/PB corona can be created in a solvent mixture cyclohexane/THF (80/20 v/v).**



**Supplementary Figure S10. TEM images of subunits and chain-like polymeric MCMs prepared from TVB terpolymers.** All samples were stained with  $\text{OsO}_4$ : black P2VP core, grey PB corona patches and PtBMA bright corona patches; scale bars are 200 nm and 25 nm in insets except (e): 5  $\mu\text{m}$  and 200 nm in inset. **(a)** TVB1 subunits with a P2VP core and a patchy corona of PB and PtBMA by direct dispersion in cyclohexane/THF (80/20 v/v). **(b)** TVB1 refined subunits after annealing for 48 h at 50  $^\circ\text{C}$ . Interestingly, the corona phase separation of the subunits can be clearly visualized. The micelles exhibit a dark P2VP core and a diffuse grey PB corona before annealing, whereas 3-5 dark PB patches were observed for the annealed sample. This demonstrates enhanced corona phase separation (refinement) by annealing. **(c)** Chain-like MCMs polymers are generated by subsequent dialysis of TVB1 into the final solvent dodecane. The PtBMA patches found for the subunits must significantly rearrange during this process. **(d)** Stronger branched polymeric MCMs obtained for TVB2 and 3D network formation for TVB3 **(e)**. TEM shows worm-like MCMs in all cases despite the much larger asymmetric ratios of  $V_{\text{PtBMA}}/V_{\text{P2VP}}$  compared to SBM. This can be explained considering the drastically different polymer/polymer and polymer/solvent interactions. As derived in Eq. 3 (main manuscript), the condition  $\gamma_{AS} < \gamma_{BS}$  is fulfilled, i.e., the surface tension of P2VP towards dodecane is higher than that of PtBMA as concluded from the interaction parameters,  $\chi_{\text{P2VP,dodecane}} = 0.81 > \chi_{\text{PtBMA,dodecane}} = 0.27$  (calculated from the corresponding solubility parameters using the increment method). In the series of TVB1-3, the increasing PtBMA content leads to more branching points, but the high interfacial tensions prevent spherical growth of subunits and keep the aggregation direction preferably linear. This exemplifies an important design criterion for targeting superstructures.



**Supplementary Figure S11. Schematic representation of a spherical MCM for the case  $V_A \gg V_B$  and scaling analysis for spherical MCMs.** Spherical micelles with a patchy multi-compartment core are formed by ABC triblock terpolymers with insoluble A and B blocks if  $V_A/V_B \equiv N_A v_A / N_B v_B \gg 1$ . The micelle comprises  $p \gg 1$  chains and consists of a central core of radius,  $R_{core}$ , formed by collapsed A-chains and is decorated by multiple,  $n$ , patches formed by collapsed B-chains (see Supplementary Note 3).

**Supplementary Table S1. Terpolymer characteristics and hydrodynamic radii,  $R_h$ , of subunits and MCMs.**

Code <sup>a</sup>	Polymer <sup>b</sup>	$V_A / V_B$ <sup>c</sup>	$r_C = \frac{N_C}{N_A + N_B}$	$R_h$ , Sub-unit [nm] <sup>d</sup>	$R_h$ , MCM [nm] <sup>e</sup>
SBM1	S <sub>354</sub> B <sub>148</sub> M <sub>352</sub> <sup>80</sup>	4.20	0.70	7 ± 4	45 ± 14
SBM2	S <sub>306</sub> B <sub>151</sub> M <sub>340</sub> <sup>74</sup>	3.57	0.75	10 ± 2	42 ± 11
SBM3	S <sub>337</sub> B <sub>333</sub> M <sub>369</sub> <sup>90</sup>	1.78	0.54	11 ± 2	36 ± 8
SBM4	S <sub>660</sub> B <sub>674</sub> M <sub>350</sub> <sup>140</sup>	1.72	0.26	14 ± 4	52 ± 14
SBM5	S <sub>611</sub> B <sub>635</sub> M <sub>292</sub> <sup>127</sup>	1.69	0.23	13 ± 1	54 ± 5
SBM6	S <sub>277</sub> B <sub>333</sub> M <sub>432</sub> <sup>90</sup>	1.46	0.70	12 ± 4	37 ± 4
SBM7	S <sub>325</sub> B <sub>681</sub> M <sub>764</sub> <sup>147</sup>	0.84	0.76	15 ± 3	33 ± 7
SBM8	S <sub>363</sub> B <sub>765</sub> M <sub>389</sub> <sup>118</sup>	0.84	0.35	17 ± 3	>500
SBM9	S <sub>283</sub> B <sub>596</sub> M <sub>304</sub> <sup>92</sup>	0.84	0.35	12 ± 5	>1000
SBM10	S <sub>374</sub> B <sub>819</sub> M <sub>509</sub> <sup>134</sup>	0.80	0.43	14 ± 2	>500
SBM11	S <sub>141</sub> B <sub>345</sub> M <sub>157</sub> <sup>49</sup>	0.72	0.32	9 ± 3	>>1000
SBM12	S <sub>283</sub> B <sub>700</sub> M <sub>378</sub> <sup>105</sup>	0.71	0.38	12 ± 1	>1000
SBV	S <sub>358</sub> B <sub>378</sub> V <sub>594</sub> <sup>120</sup>	1.67	0.81	16 ± 2	36 ± 7
SBT1	S <sub>580</sub> B <sub>124</sub> T <sub>472</sub> <sup>134</sup>	8.23	0.67	14 ± 6	32 ± 4
SBT2	S <sub>520</sub> B <sub>538</sub> T <sub>343</sub> <sup>132</sup>	1.70	0.32	12 ± 2	34 ± 6
tSfBT	tS <sub>452</sub> fB <sub>513</sub> T <sub>463</sub> <sup>392</sup>	0.62	0.45	62	>>1000
TVB1	T <sub>380</sub> V <sub>307</sub> B <sub>448</sub> <sup>110</sup>	1.77	0.64	35 ± 10	>500
TVB2	T <sub>643</sub> V <sub>293</sub> B <sub>448</sub> <sup>145</sup>	3.00	0.46	39 ± 8	>>1000
TVB3	T <sub>790</sub> V <sub>286</sub> B <sub>448</sub> <sup>165</sup>	3.68	0.40	41 ± 9	>>1000
TCD	T <sub>280</sub> C <sub>135</sub> D <sub>255</sub> <sup>111</sup>	1.17	0.62	29 ± 7	>1000
NnBEO	N <sub>178</sub> nB <sub>105</sub> EO <sub>114</sub> <sup>39</sup>	1.22	0.40	27	>1000

<sup>a</sup> SBM = polystyrene-*block*-polybutadiene-*block*-poly(methyl methacrylate), SBV = polystyrene-*block*-polybutadiene-*block*-poly(2-vinylpyridine), SBT = polystyrene-*block*-polybutadiene-*block*-poly(*tert*-butyl methacrylate), TVB = poly(*tert*-butyl methacrylate)-*block*-poly(2-vinylpyridine)-*block*-polybutadiene, TCD = poly(*tert*-butyl methacrylate)-*block*-poly(2-(cinnamoyloxy)ethyl methacrylate)-*block*-poly(2-(dimethylamino)ethyl methacrylate), tSfBT = Poly(*tert*-butoxy styrene)-*block*-poly(C<sub>6</sub>F<sub>13</sub>C<sub>2</sub>H<sub>4</sub>S-ethylene)-*block*-poly(*tert*-butyl methacrylate) and NnBEO = Poly(N-isopropyl acrylamide)-*block*-poly(*n*-butyl acrylate)-*block*-poly(ethylene oxide).

<sup>b</sup> Subscripts denote the degrees of polymerization of the corresponding blocks and superscript is the exact molecular weight in kg/mol determined with <sup>1</sup>H-NMR and GPC (PDI < 1.15). <sup>c</sup> Volume fractions  $V_A$  and  $V_B$  were calculated via polymer densities. <sup>d</sup> SBM1-12, SBV and SBT subunits measured in DMAc, tSfBT in dioxane, TVB1-3 in THF/cyclohexane (80/20 v/v), TCD in isopropanol and NnBEO in water at 25 °C. <sup>e</sup> SBM1-12 measured in acetone/isopropanol (60/40 v/v), SBV in isopropanol, SBT and tSfBT in ethanol, TVB1-3 in dodecane, TCD in water pH = 10 and NnBEO in water at 45 °C.

## Supplementary Note 1

### Kinetic Study of MCM Formation by a One Step Dialysis Procedure

The exact pathway of MCM formation during dialysis from a good solvent for all blocks into a final selective solvent (or mixture) has remained unclear so far — also in the literature. An answer to this question is accompanied by experimental difficulties, i.e., to clearly monitor changes during the dialysis process. Therein, structures continuously evolve with the solvent exchange and crucial intermediates, chain rearrangements and structural transformations can be difficult to identify. Supplementary Figure S5 depicts the results for the direct dialysis of SBM3 from the good solvent THF into an acetone/isopropanol mixture (60/40 v/v), where that polymer forms well-defined "clover" MCMs, SB<sub>3</sub>, using our controlled two-step process (i.e. DMAc against acetone/isopropanol)

An analysis of the solvent composition via <sup>1</sup>H-NMR revealed a surprisingly fast solvent exchange, practically completed after only 90 min (Supplementary Fig. S5a). TEM samples prepared at specific times during this process are shown in Supplementary Figure S5b-i. During this process, distinct species can be identified where again small subunits can be found that assemble into the final MCMs, albeit with a lower quality of the final structure as discussed in detail in Supplementary Figure S6.

After 10 min (Supplementary S5b, 47 % THF remaining), micelle formation with a strongly THF-swollen PB core and a mixed PS/PMMA corona (subunits) is indicated by the observed aggregates without clearly distinguishable phases. After 20 min (Supplementary Fig. S5c, 20 % THF), isolated hamburger MCMs can be identified among a majority of single subunits. The imaged objects are already better defined, originating from an increased selectivity of the solvent mixture and decreased swelling of the blocks PS and PB. At longer dialysis times, subunits appear more developed with PB-core and PS/PMMA-corona. Supplementary Figure S5e shows a frequent example of coexisting subunits, "hamburger" MCMs and newly formed "clover" MCMs. We take this as evidence for the assembly of intermediately formed subunits into the final MCM structures. After 50 min subunits are rarely found anymore (Supplementary Fig. S5f). "Hamburger" MCMs are the predominant species after 60 min (see Supplementary Fig. S5g), whereas more "clovers" can be found after 90 min due to the increasingly diminishing solvent quality (Supplementary Fig. S5h). The latter are the dominant fraction after a complete equilibration time of 18 h (Supplementary Fig. S5i).

Importantly, compared to the two-step process involving a defined, intermediate dissolution step in DMAc, the fine structure of the MCMs herein is less defined. The fraction of "clover" MCMs is much smaller, demonstrating larger heterogeneity that is unsuitable for further self-assembly to the next higher level. We further comment on a comparison of the various preparation routes in Supplementary Note 2.

In summary, direct dialysis from a good solvent for all blocks into the final solvent mixture also illustrates the observation of subunits and their further assembly into final MCMs. The important difference to our two-step, controlled process is that *a defined equilibration in the state of subunits does not occur as the structures continue evolving with the rapid solvent exchange*. The collapse of the middle block as first component in this dialysis procedure is governed by the various interactions (solubility parameters etc.) but is also favored on account of the connection of the PB block on both sides with other polymers, leading to an enhanced tendency for phase-separation vs. e.g. being connected on one side only. On account of the less defined and fast process, the final structures are less defined as compared to our developed two-step, directed self-assembly methodology using a defined intermediate step.

## Supplementary Note 2

### Fine-Structure and Homogeneity of the MCMs Depending on the Preparation Method: Direct Dispersion vs. One Step Dialysis vs. Two Step Dialysis

A well-defined monodisperse structuring of the MCMs is of great importance for colloidal superstructure formation. This section addresses the advantages of our two-step approach vs. previous methods. Therefore, we compare the resulting MCM fine structures of different polymers as a function of the preparation pathway: (a) direct dispersion in the final solvent, (b) dialysis from a good solvent for all blocks into the final solvent (termed: one step dialysis, see Supplementary Fig. S5), and (c) step-wise reduction of conformational degrees of freedom using an intermediate step in a selective solvent for both A and C (termed: two step dialysis).

As depicted in Supplementary Figure S6 "football" MCMs, as formed by SBM2 (Supplementary Fig. S6a1-a3), represent the most reported MCM example in the literature<sup>14,15,17,47,49</sup> and probably are the thermodynamically most robust morphology. This structure can be obtained for a suitable polymer (SBM2) for all three preparation techniques investigated. The large fraction of the soluble PMMA block helps maintaining dynamics and facilitates their preparation even via direct dissolution.

Significant differences occur in case of SBM3, SBM6, and SBM9, which form uncommon and more labile morphologies. Direct dispersion of the terpolymers only leads to "football" MCMs or even more ill-defined structures (Supplementary Fig. S6b1, c1 and d1). The polydispersity of the fine structure and overall size-distribution increases as compared to SBM2. The rather exceptional "clover", "hamburger", or chain-like MCM morphologies are exclusively obtained via the two step dialysis as shown in Supplementary Fig. S6b2-d2 and S6 b3-d3.

Further evaluation of the inner fine structure reveals important differences between direct dialysis from a common solvent to the two step procedure using DMAc as intermediate solvent. Although qualitatively the same structures can be obtained, the fine structure is significantly more developed in case of the more controlled two step approach using the DMAc step. Therein, "clover" and "hamburger" MCMs are almost exclusively observed (Supplementary Fig. S6b3 and c3).

Additionally, the one step dialysis procedure results in a higher polydispersity of the aggregates (Supplementary Fig. S6b2 and c2). For instance, SBM6 exhibits almost equal fractions of subunits, "hamburger" and "clover" MCMs, thus not corresponding to a well-defined structure formation. Similarly, the worm-like MCMs (Supplementary Fig. S6d2) show much higher branching, originating from structural inhomogeneities of the underlying MCM monomers. Hence, quantitative differences between the procedures are evident.

These effects are not specific to a particular triblock terpolymer system. Similar behavior can be observed for SBT and SBV polymers (Supplementary Fig. S6e1-e3, f1-f3), for which highest homogeneity can again only be obtained for the two step dialysis.

*Consequently, homogeneous populations of complex MCM morphologies may not be accessible using direct dispersion or fast one step dialysis, but essentially require a control of the pathway as exercised via our controlled/dedicated process. As expected, this problem is more pronounced for larger fractions of solvophobic blocks, meaning reduced overall dynamics for structural rearrangements.*

To further underscore the importance of maintaining dynamics, Supplementary Figure S6g1-3 and h1-3 show results obtained for the self-assembly of TCD at pH = 6 and pH = 10 in water. In con-

trast to the other previously shown polymers in organic solvents, water serves as final solvent for TCD. Due to its unique solvent properties, H<sub>2</sub>O suppresses dynamics of solvophobic (here hydrophobic) segments for amphiphilic triblock terpolymers more efficiently than organic solvents in case of solvophobic blocks. Therefore, the kinetic obstacles are more pronounced and even larger differences between the three methods can be observed. Direct dispersion completely fails at both pH values in the observed time frame of one week. The solution stays macroscopically phase-separated and only some micron-scale ill-defined aggregates can be found. Secondly, the one step dialysis (as would commonly be applied to such polymers) leads to nanosized aggregates, but a distinct nanostructuration cannot be observed. The polydispersity of these aggregates increases significantly when using alkaline water (pH = 10) as compared to water with pH = 6. This can again be understood considering the better solubility of the D corona chains upon slight protonation at pH = 6 and the therewith higher dynamics.

In strongest contrast to these methods, the two step dialysis furnishes well-defined nanostructured aggregates whose degree of aggregation into linear chains can be changed by the pH value. Such an unprecedented control is not achievable without distinct and precise control of the self-assembly pathway.

*In conclusion, these important results convincingly demonstrate the advantage of an intermediate reduction of the degrees of conformational freedom in a first solvent (e.g. DMAc), leading to well-defined key subunits and, in turn, drastically improved control over structure and polydispersity of the final MCMs. Moreover, fine structures are accessible with the two step process that remain inaccessible using previous state-of-the-art dispersion methods.*

### Supplementary Note 3

#### Scaling analysis for spherical MCMs

The corona of the MCM is formed by solvated C chains protruding from the B-domains (patches) into the solution. Even though scaling arguments<sup>49,59-61</sup> presented below are strictly applicable in the range of  $n \gg 1$ , the results can be extrapolated to the  $n \geq 1$  case. The free energy (in  $k_B T$  units) of the MCM can be presented as

$$F = F_{\text{corona}} + F_{\text{core}} + F_{\text{interface}} \quad (\text{S1})$$

where  $F_{\text{corona}}$  describes repulsive interactions (under good or theta-solvent conditions) between solvated and crowded coronal chains C, whereas  $F_{\text{core}}$  accounts for the conformational entropy losses in the collapsed core-forming segments: This term is negligibly small as long as the aggregates retain a spherical shape. The last term,  $F_{\text{interface}}$ , accounts for the excess free energy of the interfaces between collapsed B and A segments and solvent, as well as that of the interfaces between B and A domains:

$$F_{\text{interface}} = F_{AS} + F_{BS} + F_{AB} = \gamma_{AS} S_{AS} + \gamma_{BS} S_{BS} + \gamma_{AB} S_{AB} \quad (\text{S2})$$

where  $S_{AS}, S_{BS}, S_{AB}$  are the interfacial areas and the surface tension at the A/S (S=solvent), B/S, and B/A interfaces in  $k_B T$  units equals  $\gamma_{AS}, \gamma_{BS}, \gamma_{AB}$ , respectively.

The equilibrium aggregation number,  $p$ , and the number of B-domains (patches) in one MCM can be found from minimization of the free energy of the MCM calculated per chain.

The interfacial free energy (Eq. S2) can be presented in the form

$$F_{\text{interface}} = \gamma_{BS} S_{BS} + (\gamma_{AB} - \gamma_{AS}) S_{AB} + \gamma_{AS} (S_{AS} + S_{AB}) = \Delta F_{\text{interface}} + 4\pi R_{\text{core}}^2 \gamma_{AS} \quad (\text{S3})$$

where

$$4\pi R_{\text{core}}^2 = S_{AS} + S_{AB} = (4\pi)^{1/3} 3^{2/3} (pV_A)^{2/3} \quad (\text{S4})$$

is the total interfacial area of the spherical A-core and

$$\Delta F_{\text{interface}} = \gamma_{BS} (S_{BS} - S_{AB} \cos \theta) \quad (\text{S5})$$

where  $\cos \theta = (\gamma_{AS} - \gamma_{AB}) / \gamma_{BS}$  is the cosine of the contact angle formed by B-domains with the A/S interface. Here we neglect the curvature of the central A-core as compared to that of the B-patches. This is justified provided  $\gamma_{AB} \gg \gamma_{AS} - \gamma_{BS}$  corresponding to dewetting of B-domains from the A/S interface. The latter condition implies instability of a laterally uniform core-shell-corona structure with respect to formation of patchy MCMs.

Assuming that each B-domain (one patch) comprises  $m = p / n$  chains, Eq. S5 can be presented as

$$\Delta F_{\text{interface}} = (2\pi)^{1/3} 3^{2/3} \gamma_{BS} (mV_B)^{2/3} n \left(1 + \frac{\cos \theta}{2}\right)^{1/3} (1 - \cos \theta)^{2/3} \quad (\text{S6})$$

The total interfacial free energy can be presented as

$$F_{\text{interface}} = (2\pi)^{1/3} 3^{2/3} \tilde{\gamma}_{BS} (mV_B)^{2/3} n + 6^{2/3} \pi^{1/3} \gamma_{AS} (pV_A)^{2/3} \quad (\text{S7})$$

with the notation

$$\tilde{\gamma}_{BS} \approx \gamma_{BS} (1 - \cos \theta)^{2/3} \left(1 + \frac{\cos \theta}{2}\right)^{1/3} \quad (\text{S8})$$

Finally, the interfacial free energy per chain can be presented as

$$\frac{F_{\text{interface}}}{p} \approx \tilde{\gamma}_{BS} m^{-1/3} V_B^{2/3} + \gamma_{AS} p^{-1/3} V_A^{2/3} \quad (\text{S9})$$

where we have omitted numerical factors of the order of unity in the last expression.

The corona contribution to the free energy should be specified separately for starlike and for the crew-cut micelles.

**For starlike micelles,**  $d_{\text{corona}} \equiv R_{\text{micelle}} - R_{\text{core}} \gg R_{\text{core}}$ , the free energy of the corona (per chain) can be presented as

$$\frac{F_{\text{corona}}}{p} = m^{1/2} \ln \frac{R_{\text{core}}}{R_B n^{1/2}} + p^{1/2} \ln \frac{R_{\text{micelle}}}{R_{\text{core}} (1 + n^{-1/2})} \quad (\text{S10})$$

The first term in Eq. S10 describes steric interactions between segments of the C-chains, which are confined between the B-patches within the core region of width  $h_{\text{patch}} \sim R_{\text{core}} n^{-1/2}$ . Here, we also introduced the characteristic size of a B-patch  $R_B \approx (mV_B)^{1/3} \ll R_{\text{core}} n^{-1/2}$ . The second term in Eq. S10 accounts for steric interactions in the peripheral regions of the corona, i.e., at distances from the core surface exceeding  $h_{\text{patch}}$ . Remarkably, Eq. S10 applies both under good and theta-solvent conditions for the corona chains. The outermost radius of the corona,  $R_{\text{corona}}$ , is given by

$$R_{corona} \cong \begin{cases} \ell N_C^{3/5} \tau_C^{1/5} p^{1/5}, & \text{for good solvent} \\ \ell N_C^{1/2} p^{1/4}, & \text{for near-}\Theta \text{ solvent} \end{cases} \quad (\text{S11})$$

Minimization of the free energy of the micelle given by Eqs. S1, S9, S10 with respect to  $m$  and  $p$  enables us to derive the total aggregation number and the number of patches in the equilibrium spherical starlike MCMs.

The total aggregation number

$$p \cong (N_A v_A)^{4/5} \gamma_{AS}^{6/5} \ln^{-6/5} (R_{micelle} / R_{core}) \quad (\text{S12})$$

in spherical starlike MCMs is controlled by the balance of the interfacial energy of the core and the contribution to the free energy of the coronal regions at a distance from the core exceeding the distance between the centers of adjacent patches,  $h_{patch}$

Here, the core radius  $R_{core} \cong (p N_A v_A)^{1/3} \cong (N_A v_A)^{3/5} \gamma_{AS}^{2/5}$  and the micellar radius are

$$R_{micelle} \cong \begin{cases} \ell N_C^{3/5} \tau_C^{1/5} (N_A v_A)^{4/25} \gamma_{AS}^{6/25}, & \text{for good solvent} \\ \ell N_C^{1/2} (N_A v_A)^{1/5} \gamma_{AS}^{3/10}, & \text{for near-}\Theta \text{ solvent} \end{cases} \quad (\text{S13})$$

The number of patches (B-domains) is given by

$$n \cong (N_A v_A / N_B v_B)^{4/5} (\gamma_{AS} / \tilde{\gamma}_{BS})^{6/5} \ln^{-6/5} (R_{micelle} / R_{core}) \quad (\text{S14})$$

The number of patches is controlled primarily by the ratio  $N_A v_A / N_B v_B$  of volumes of the core-forming blocks and weakly (logarithmically) decreases as a function of length and solvent quality for the corona-forming block C. As stated above, MCMs with multiple B-patches decorating a central A-core are formed by asymmetric terpolymers with  $N_A v_A / N_B v_B \gg 1$ .

**For the crew-cut micelle,**  $h_{patch} \ll d_{corona} \ll R_{core}$ , the first term in Eq. S10, corresponding to the contribution from the inter-patch regions, remains the same, whereas in the periphery of the corona the curvature effects are negligible and the distal regions of the corona can be assimilated to a planar polymer brush with the average area C-chain  $s \approx R_{core}^2 / p$ . Remarkably, at  $n \gg 1$  the majority of the monomer units of the C-blocks are located in the distal (quasi-planar) region of the corona. The free energy per chain in a planar brush scales as

$$\frac{F_{brush}}{p} \cong \begin{cases} N_C \tau_C^{1/3} (s / \ell^2)^{-5/6}, & \text{for good solvent} \\ N_C (s / \ell^2)^{-1}, & \text{for near-}\Theta \text{ solvent} \end{cases} \quad (\text{S15})$$

and the coronal free energy (per chain) for the crew-cut MCM can be presented as

$$\frac{F_{corona}}{p} \cong m^{1/2} \ln \frac{R_{core}}{R_B n^{1/2}} + \begin{cases} N_C \tau_C^{1/3} p^{5/18} N_A^{-5/9}, & \text{for good solvent} \\ N_C p^{1/3} N_A^{-2/3}, & \text{for near-}\Theta \text{ solvent} \end{cases} \quad (\text{S16})$$

Minimization of the free energy of the micelle given by Eqs. S1, S9, S16 with respect to  $m$  and  $p$  enables us to find the total aggregation number and the number of patches in the crew-cut MCM. The result is given by

$$p \cong \begin{cases} (\gamma_{AS} \ell^2 / N_C \tau_C^{1/3})^{18/11} (N_A v_A)^2 \ell^{-6}, & \text{for good solvent} \\ (\gamma_{AS} \ell^2 / N_C)^{3/2} (N_A v_A)^2 \ell^{-6}, & \text{for near-}\Theta \text{ solvent} \end{cases} \quad (\text{S17})$$

and

$$n \cong (N_A v_A)^2 (N_B v_B)^{-4/5} \tilde{\gamma}_{BS}^{-6/5} \cdot \begin{cases} (\gamma_{AS} / \ell^{5/3} N_C \tau_C^{1/3})^{18/11}, & \text{for good solvent} \\ (\gamma_{AS} / \ell^2 N_C)^{3/2}, & \text{for near-}\Theta \text{ solvent} \end{cases} \quad (\text{S18})$$

Similarly to the case of starlike micelles, the number of patches increases with  $V_A / V_B \equiv v_A N_A / v_B N_B$  and decreases with the solvent strength,  $\tau_C$ , and the length,  $N_C$ , of the coronal block.

Eqs. S17, S18 apply as long as  $h_{patch} \leq d_{corona}$ , i.e., the area of the A-core between the patches is protected by the corona. This is the case provided that

$$\begin{cases} N_C \tau_C^{1/3} \geq (N_B v_B)^{11/15} \gamma_{BS}^{11/10} \gamma_{AS}^{-5/6} \ell^{-5/3}, & \text{for good solvent} \\ N_C \geq (N_B v_B)^{4/5} \gamma_{BS}^{6/5} \gamma_{AS}^{-1} \ell^{-2}, & \text{for near-}\Theta \text{ solvent} \end{cases} \quad (\text{S19})$$

If condition of Eq. S19 is violated, the crew-cut MCMs are expected to be instable and further aggregation or superstructure formation occurs.

### Core morphology

We first consider starlike micelles formed by terpolymers with nearly symmetrical core-forming blocks,  $N_A v_A / N_B v_B \approx 1$ , (for  $N_A v_A / N_B v_B \ll 1$  the collapse of the A-domains does not lead to any significant change in the aggregation number as compared to the ‘‘precursor’’ micelle with a mixed A/C corona; further, this does not lead to aggregation of the precursor micelles. According to Eq. S14 the number of B-domains is of the order of unity, though the scaling approach does not enable us to specify the exact number of patches, e.g., to distinguish between  $n = 2$  (‘‘double burger’’) and  $n = 1$  (‘‘inverse hamburger’’) cases. Since in the starlike micelle,  $d_{corona} = R_{micelle} - R_{core} \gg R_{core}$ , the dominant contribution to the free energy of the corona does not depend on the details of the structure of the compartmentalized core, here we compare the overall interfacial free energies of BAB and ABA structures<sup>62</sup>. For simplicity, we assume that  $\gamma_{AS} \gamma_{BS} \gg \gamma_{AB}$  and, as a result, the compartmentalized core has an overall spherical shape with either one (central) B domain and two A domains or with one central A domain and two B domains.

Then the interfacial free energy can be presented as

$$F_{interface}^{(ABA)} = \gamma_{AS} S_{AS} + \gamma_{BS} S_{BS} + \gamma_{AB} S_{AB} = 4\pi R_{core}^2 [\gamma_{BS} + (\gamma_{AB} + \gamma_{AS} - \gamma_{BS})x - \frac{1}{2}\gamma_{AB}x^2] \quad (\text{S20})$$

where  $R_{core} = [3p(V_A + V_B) / 4\pi]^{1/3}$  is the core radius and  $x$  is the root of the equation

$$x^2 - \frac{1}{3}x^3 = \frac{2}{3} \cdot \frac{V_A}{V_A + V_B} \quad (\text{S21})$$

and similarly for the BAB shape of the core. For nearly symmetrical composition,  $|(V_A / V_B) - 1| \ll 1$  the sign of the difference in the free energies,  $F_{interface}^{(ABA)} - F_{interface}^{(BAB)}$ , only depends on the ratio of volumes of insoluble blocks,  $V_A / V_B$  and on the combination of interfacial tensions,  $(\gamma_{AS} - \gamma_{BS}) / \gamma_{AB}$ . Specifically, the ABA shape of the core corresponds to lower interfacial free energy than the BAB shape if

$$V_A / V_B \leq [1 + const \cdot (\gamma_{AS} - \gamma_{BS}) / \gamma_{AB}]^{-1} \quad (\text{S22})$$

where the numerical constant is of the order of unity.

## Supplementary References

- <sup>59</sup> Halperin, A. & Alexander, S. Polymeric micelles: Their relaxation kinetics. *Macromolecules* **22**, 2403-2412 (1989).
- <sup>60</sup> Birshtein, T. M. & Zhulina, E. B. Scaling theory of supermolecular structures in block copolymer-solvent systems: 1. Model of micellar structures. *Polymer* **30**, 170-177 (1989).
- <sup>61</sup> Zhulina, E. B. & Borisov, O. V. Scaling Theory of 3-Miktoarm ABC Copolymer Micelles in Selective Solvent. *Macromolecules* **41**, 5934-5944 (2008).
- <sup>62</sup> Cates, M. E. & Candau, S. J. Statics and dynamics of worm-like surfactant micelles *J. Phys.: Condens. Matter* **2**, 6869 (1990).